Solid-State Electronics 136 (2017) 3–11

Contents lists available at ScienceDirect

Solid-State Electronics

journal homepage: www.elsevier.com/locate/sse

A review of the synthesis of reduced defect density $In_xGa_{1-x}N$ for all indium compositions

Evan A. Clinton [a], Ehsan Vadiee [a], Chloe A.M. Fabien [a], Michael W. Moseley [a], Brendan P. Gunning [a], W. Alan Doolittle [a,*], Alec M. Fischer [b], Yong O. Wei [b], Hongen Xie [b], Fernando A. Ponce [b]

[a] School of Electrical and Computer Engineering, Georgia Institute of Technology, Atlanta, GA 30332, USA
[b] Department of Physics, Arizona State University, Tempe, AZ 85287, USA

ARTICLE INFO

Article history:
Available online 24 June 2017

The review of this paper was arranged by A. A. Iliadis, A. Akturk, R. P. Tompkins, and A. Zaslavsky

ABSTRACT

A review of metal rich and nitrogen rich (N-rich), low-temperature grown $In_xGa_{1-x}N$ is provided, focusing on two low-temperature approaches that have resulted in non-phase separated $In_xGa_{1-x}N$. The metal modulated epitaxy (MME) and N-rich, low temperature approaches to the reduction of defects in $In_xGa_{1-x}N$ are described and are capable of growing $In_xGa_{1-x}N$ throughout the miscibility gap. MME films remain smooth at all thicknesses but show device quality material primarily for $x < 0.2$ and $x > 0.6$. Low temperature, N-rich grown films show a critical thickness extend well beyond the theoretical values and results in slower relaxation through the $0.2 < x < 0.6$ range most interesting for light emitters and solar cells. This reduced defect density results in improved optical emission, but due to increased roughening with increased thickness, low temperature, N-rich films are limited to thin layers. Future thick $In_xGa_{1-x}N$ substrates are necessary to increase design freedom, as well as improve optoelectronic device performance. Initial results with films up to 800 nm are shown to display evidence of defect annihilation which could be promising for future thick optoelectronic templates and thick devices.

1. Introduction

Group III-nitrides have been thoroughly investigated due to notable material characteristics relevant to many power electronic and optoelectronic applications [1–5]. A direct bandgap semiconductor between ~0.7 and 6.1 eV can be formed when alloying InN, GaN, and AlN [6]. Additionally, high absorption coefficients, radiation resistances, and carrier mobilities are some further benefits of the III-nitrides [7].

The $In_xGa_{1-x}N$ alloy has been the subject of more recent research efforts towards optoelectronics because of its tunable direct bandgap between InN at ~0.7 eV and GaN at ~3.4 eV, which conveniently spans from infrared, through visible, and into ultraviolet wavelengths [6]. Thus, $In_xGa_{1-x}N$ is actively used for light emitting diodes (LEDs), lasers, and is being considered for photovoltaics [2]. The former LED efforts by Nakamura, Amano, and Akasaki resulted in a Nobel prize in physics in 2014 [8].

Although $In_xGa_{1-x}N$ bearing devices such as the blue LED have been successfully commercialized, the active $In_xGa_{1-x}N$ layer is typically a small volume of the device in the form of quantum wells and is a low mole fraction of indium [8]. Metal-organic chemical vapor deposition (MOCVD) has been the preferred tool for growing these LED structures [8]. Unfortunately, indium incorporation above 20% becomes difficult at the elevated growth temperatures necessary for MOCVD, while molecular beam epitaxy (MBE) can incorporate indium and grow $In_xGa_{1-x}N$ of all compositions from $0 < x < 1$ [9].

While indium incorporation tends to be easier for MBE growth of $In_xGa_{1-x}N$ alloys, many difficulties still exist with the growth of these films. Higher indium content $In_xGa_{1-x}N$ becomes increasingly difficult to grow due to phase separation [9] originating from growth kinetics such as the thermal decomposition of InN bonds as well as indium surface segregation [10]. Furthermore, including high indium content films into device structures requires device designs that either avoid or annihilate defects generated from the lattice-mismatched interface between the $In_xGa_{1-x}N$ film and the substrate or underlying layer, which is most commonly GaN. These unfortunate growth phenomena have prevented researchers from realizing an assortment of device structures that require high quality and high indium content films, such as an efficient green LED and solar cells.

It has been suggested that phase separation is driven by intrinsic properties of $In_xGa_{1-x}N$, specifically spinodal decomposition [11]. However, this mechanism involves bulk diffusion of constituent atoms which is remarkably difficult in all III-nitrides,

* Corresponding author.
E-mail address: alan.doolittle@ece.gatech.edu (W.A. Doolittle).

http://dx.doi.org/10.1016/j.sse.2017.06.020
0038-1101/

$In_xGa_{1-x}N$ included. Thus, prior work has alternatively suggested that phase separation is largely driven by metallic surface diffusion and decomposition effects [10]. For this reason, methods that can vary the diffusion rate of metal adatoms are useful for producing non-phase separated $In_xGa_{1-x}N$. These methods can be chemical, by supplying an excess of metal to enhance surface diffusion via weak metallic bonds, or thermal, by limiting diffusion with a decreased substrate temperature. In this way, the kinetics of adatom incorporation are the dominant factor in producing non-phase separated $In_xGa_{1-x}N$. While other reviews of $In_xGa_{1-x}N$ have been undertaken [12,13], two promising methods remain poorly understood. Therefore, this review focuses on metal rich and nitrogen-rich (N-rich), low temperature growth methods.

The metal modulated epitaxy (MME) growth technique can overcome some of the challenges associated with growing non-phase separated $In_xGa_{1-x}N$ alloys [10]. MME involves shuttering group III metals with a constant nitrogen plasma supply, as seen in Fig. 1, to toggle between N-rich growth and metal rich growth while continuously growing unlike some cyclical flux techniques. Critically, this is performed at low enough temperatures to avoid the intermediate growth regime most often used for MBE epitaxy [14]. MME allows a film to benefit from properties facilitated by the metal rich growth regime such as a higher adatom mobility, and also to benefit from the advantages of N-rich growth such as dramatically higher magnesium incorporation and activation for p-type doping [10,15–19]. Transient reflection high energy electron diffraction (RHEED) signals and RHEED patterns allow for *in-situ* feedback on the buildup of metallic layers, the roughness of the film, the III/V ratio, and the growth rate [10]. MME has shown the ability to grow non-phase separated $In_xGa_{1-x}N$ throughout the entire compositional range [20].

In this review, the MME growth technique is first examined followed by a summary of low temperature grown, N-rich $In_xGa_{1-x}N$. The growth of both MME and N-rich $In_xGa_{1-x}N$ films throughout the compositional range and each techniques' advantages and disadvantages will be evaluated [22,23]. High indium content solar cells grown using the low temperature N-rich method will be discussed, and finally pathways towards improving future devices containing $In_xGa_{1-x}N$ will be presented [24,25].

2. Experimental setup

Samples in this review were grown in a Riber 32 MBE chamber. A standard effusion cell was used for aluminum, indium, silicon, and germanium while a Veeco dual filament hot-lip SUMO cell was used for the gallium source. A Veeco corrosive-series valved cracker operating at a bulk temperature of 280–330 °C and a tip temperature of 900 °C was used for the magnesium source as originally described elsewhere [26]. A Veeco Unibulb standard and high conductance plasma source was operated at different conditions to enable high growth rate but was most commonly operated at 350 W and 2–4 sccm nitrogen flow rate. Growths were initiated on either MOCVD-grown GaN templates or sapphire. All samples were sputtered with ~2 μm of tantalum on the backside to ensure thermal uniformity during growth. Before starting the growths, the samples were cleaned with a piranha etch of H_2SO_4:H_2O_2 (3:1) at 150 °C. Samples were then outgassed in an introductory chamber at 200 °C for 20 min.

GaN buffer layers were first grown on samples with GaN templates, while sapphire samples were nitrided and then AlN followed by GaN buffer layers were grown according to the procedure described by Namkoong et al. [27] and Losurdo et al. [28]. $In_xGa_{1-x}N$ films were grown from 300 to 600 °C with target compositions chosen by varying the indium to gallium ratio and adjusting flux ion gauge readings weighted by the atomic Z-number. For MME growths, both the gallium and indium shutters were toggled simultaneously, while the active nitrogen from the plasma is constantly being supplied, as seen in Fig. 1.

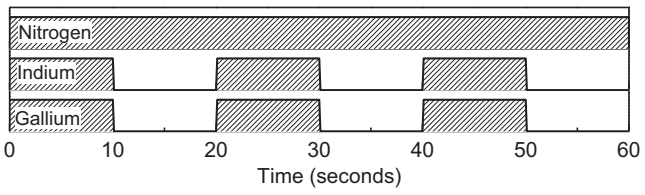

Fig. 1. Shuttering sequence for MME $In_xGa_{1-x}N$ [21].

3. Results and discussion

3.1. Surface kinetics and in-situ feedback of MME GaN

Since the MME growth of ternaries is considerably more complex than that of binaries, a representative baseline is first established for the growth of binaries. MME is a low temperature, desorption free growth technique that involves shuttering the group-III sources and dopant cells while applying a constant flux of active nitrogen species, illustrated in Fig. 2. By operating at low temperatures with metal fluxes 2–3 times the stoichiometric point, the intermediate phase regime where surface pits are often formed is avoided, while still growing very fast up to 9.8 μm/h [29], high quality films [16].

The metal modulated epitaxy growth technique has been demonstrated to improve material quality of GaN [15,19], AlN [30,31], and InN films [32]. MME of GaN films can allow for extremely high dopant concentrations for germanium and silicon n-type GaN up to $\sim 1 \times 10^{20}$ electrons/cm^3 and magnesium doped p-type GaN up to $\sim 7 \times 10^{19}$ holes/cm^3 [18].

RHEED intensity signals and patterns are used *in-situ* to determine III/V ratio and to gauge the metal buildup on the surface and the roughness of the film. All three binary alloys show nearly identical RHEED signatures, so only GaN is discussed herein. This RHEED feedback is convenient because any fluctuation in stoichiometry can be adjusted and thus controlled during a growth. The growth of unintentionally doped (UID) and n-type doped films typically have smooth 2×2 reconstructed RHEED patterns, and accompanying low roughness of ~0.2 nm RMS, as measured by atomic force microscopy (AFM), as seen in Fig. 3(b) and (c), respectively [29]. These smooth films are achievable with high III/V ratios of $1.8 < III/V < 3$ with shutter open and closed times around 10 s.

MME of p-type GaN is performed at a slightly different III/V ratio of ~1.2–1.3 which might prevent nitrogen vacancies (V_N) to form which act as donors when growing more metal rich [18]. This III/V ratio when combined with a 5 s shutter open time and a 10 s shutter closed time can result in hole concentrations $\sim 7 \times 10^{19}$ holes/cm^3 [17]. These p-type growth conditions tend to result in

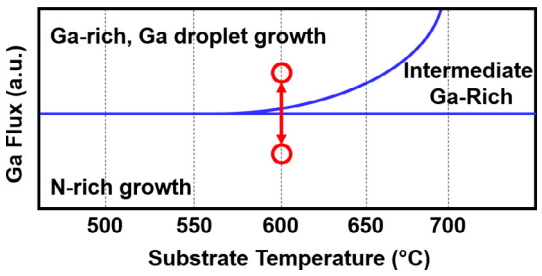

Fig. 2. Growth diagram of MME GaN indicating the typical substrate temperature and shuttering technique to transition between Ga-rich and N-rich growth regimes.

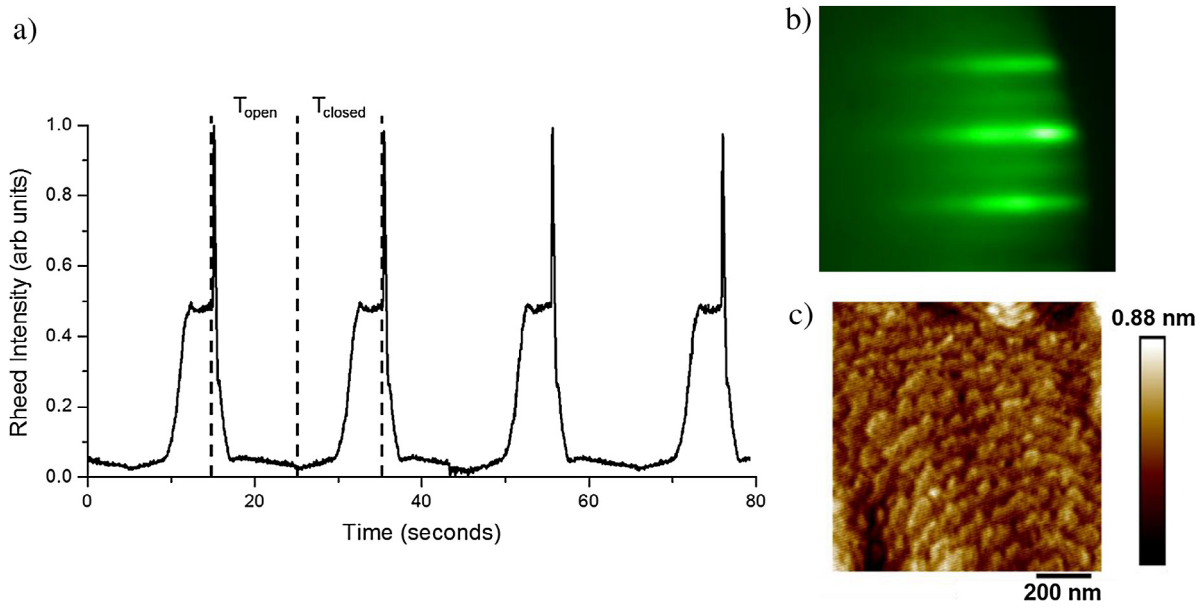

Fig. 3. (a) Transient RHEED signal with shutter open and closed times labelled, (b) RHEED pattern during growth exhibiting a 2×2 reconstruction pattern indicating a smooth surface, and (c) post-growth 1 μm × 1 μm AFM scan of a UID MME GaN film showing step-flow growth with roughness of 0.09 nm RMS and a height scale of 0.88 nm.

an AFM roughness of 1–2 nm RMS. Similarly to the UID and n-type growth conditions, RHEED acts as an *in-situ* feedback source. Fig. 2 illustrates how a lower III/V ratio combined with a lower shutter open time results in a lower metal dose (downward transient not completed before the shutter is closed), and thus a slightly higher roughness (increasing RHEED intensity with time indicates increasing roughness).

The results shown in Figs. 3 and 4 illustrate how with calibrated growth conditions, MME of UID, n-type, and p-type GaN can be a routine and repeatable procedure with *in-situ* feedback from RHEED. For more in-depth information on the growth kinetics of MME GaN and p-type GaN refer to Moseley et al. [16] and Gunning et al. [18].

3.2. Surface kinetics and in-situ feedback of MME $In_xGa_{1-x}N$

MME of $In_xGa_{1-x}N$ films requires extra attention to RHEED intensity signals in order to observe surface kinetics such as thermal decomposition and indium surface segregation that result in phase separation [10]. Some amount of phase separation in $In_xGa_{1-x}N$ LEDs can be tolerated because higher indium content clusters result in localized concentrations of carriers and improve

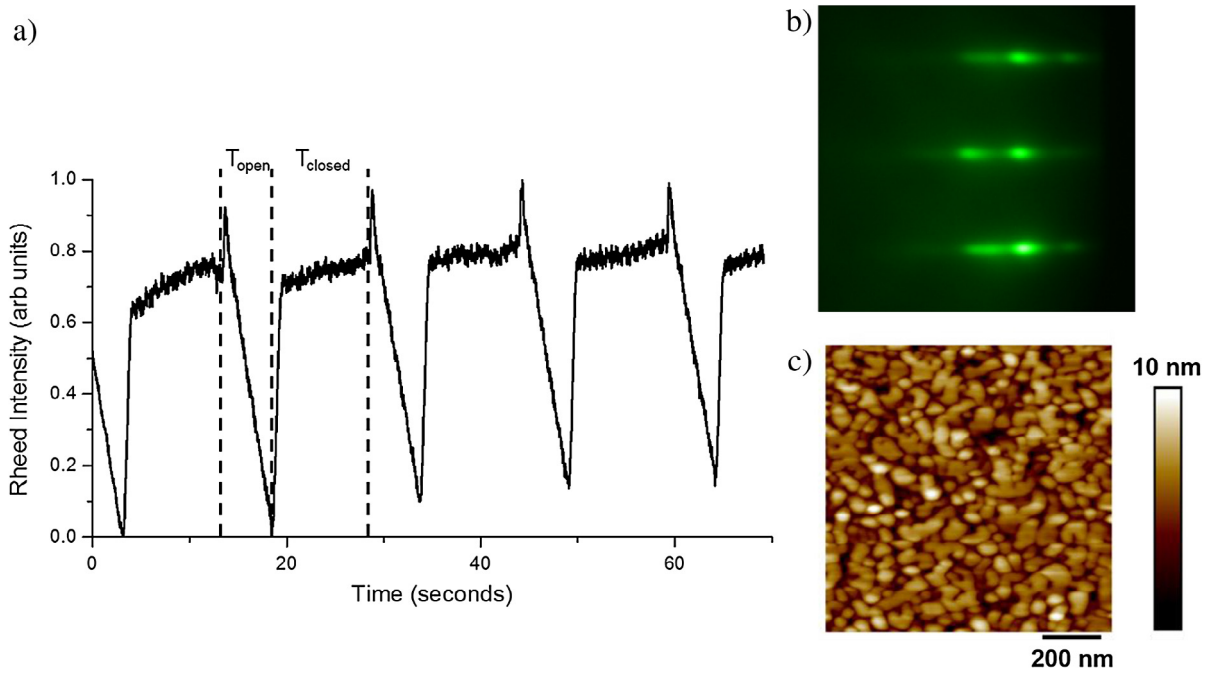

Fig. 4. (a) Transient RHEED signal with shutter open and closed times labelled, (b) RHEED pattern during growth exhibiting a streaky-smooth 1×1 reconstruction pattern, and (c) post-growth 1 μm × 1 μm AFM scan of a p-type MME GaN film with a roughness of 1.14 nm RMS and a height scale of 10 nm.

radiative emission. Other devices such as solar cells require uniform $In_xGa_{1-x}N$ films to increase carrier collection efficiency [33,34]. In order to improve these devices' performance, growth techniques must be capable of either mitigating (for solar cells) or controlling the degree of (for LEDs) phase separation in $In_xGa_{1-x}N$. Low substrate temperature tends to reduce thermal decomposition and nitrogen rich growth eliminates the surface segregation effect [35,36], but both of these conditions lower adatom mobility and thus result in rougher films. Metal rich growth tends to improve film quality but results in indium surface segregation. MME can be a suitable alternative to this dilemma.

Phase separation due to surface segregation of indium metal occurs in the metal rich regime where indium migrates to the surface of the accumulated indium and gallium metallic adlayer(s) [10]. The surface segregated indium can ride on the surface of metal rich films throughout the duration of the film's growth. The indium is then nitrided when the film is cooled down. The result is an InN surface layer with an indium depleted $In_xGa_{1-x}N$ layer as seen in the upper X-ray diffraction scan of Fig. 5.

Phase separation from thermal decomposition of InN bonds occurs due to thermal energy from the substrate temperature breaking InN bonds [10]. At the conclusion of the growth, residual indium on the surface that has not desorbed can form InN on the surface due to nitridation during the cool down stage, as seen in the middle sample of Fig. 5. Thermal decomposition at the end of the growth can be eliminated by capping the film with GaN, as seen in the lower sample of Fig. 5. Furthermore, if the substrate temperature is high enough, thermal decomposition can prevent growth entirely [37].

Mitigating phase separation entirely in MME $In_xGa_{1-x}N$, as seen in the lower sample of Fig. 5, is possible by controlling the indium dose and capping the structure with GaN to prevent thermal decomposition upon cooldown [10]. Surface segregation and thermal decomposition are exacerbated at higher indium compositions because single phase growth requires lowering the metal dose and the substrate temperature to avoid each mechanism, respectively. For further details into the RHEED transients and surface kinetics during MME $In_xGa_{1-x}N$ growth, refer to Moseley et al. [10,22].

3.3. MME $In_xGa_{1-x}N$ films throughout the miscibility gap

Smooth, single phase $In_xGa_{1-x}N$ films of all compositions from $0 \leq x \leq 1$ can be grown via MME [22]. Results demonstrating this capability are shown in Fig. 6. These films were grown between 400–450 °C and at a metal rich condition upon opening the metal shutters, but with shutter open times short enough to not exceed the critical dose for indium surface segregation [10]. The X-ray diffraction scans have pendellösung fringe peaks which arise from interfacial interference, and can be used to calculate the $In_xGa_{1-x}N$ film thickness. These films are all around 50 nm thick and have GaN caps to prevent thermal decomposition. Each sample in Fig. 6 demonstrates roughness values <1 nm RMS and X-ray (0002) symmetric rocking curve full width at half maximum (FWHM) values of 360–420 arcsecs.

Transmission electron microscopy (TEM) was performed on some of these MME $In_xGa_{1-x}N$ samples [38]. Cross-section TEM along the $11\bar{2}0$ direction is shown in Fig. 7. The lowest indium content film with x = 0.22 shows many stacking faults. Next, the x = 0.46 film demonstrates granular features. At x = 0.60, the $In_xGa_{1-x}N$/GaN upper and lower interfaces are populated with misfit dislocations marked by moiré fringes due to the large lattice mismatch between the $In_xGa_{1-x}N$ film and the GaN layers. Finally, the highest indium composition film at x = 0.67 also exhibits moiré fringes. The misfit dislocations immediately relax the $In_xGa_{1-x}N$

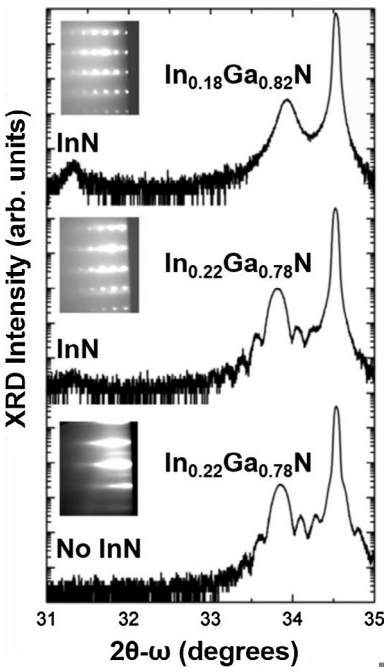

Fig. 5. X-ray diffraction and RHEED inset images of MME grown $In_xGa_{1-x}N$ films on GaN. The top film exhibits phase separation due to surface segregation of excess indium during metal rich growth. The middle film exhibits phase separation from thermal decomposition of InN bonds during the cool down stage after growth. The bottom film does not exhibit phase separation, which is possible by controlling the $In_xGa_{1-x}N$ metal dose and capping the film with GaN [22].

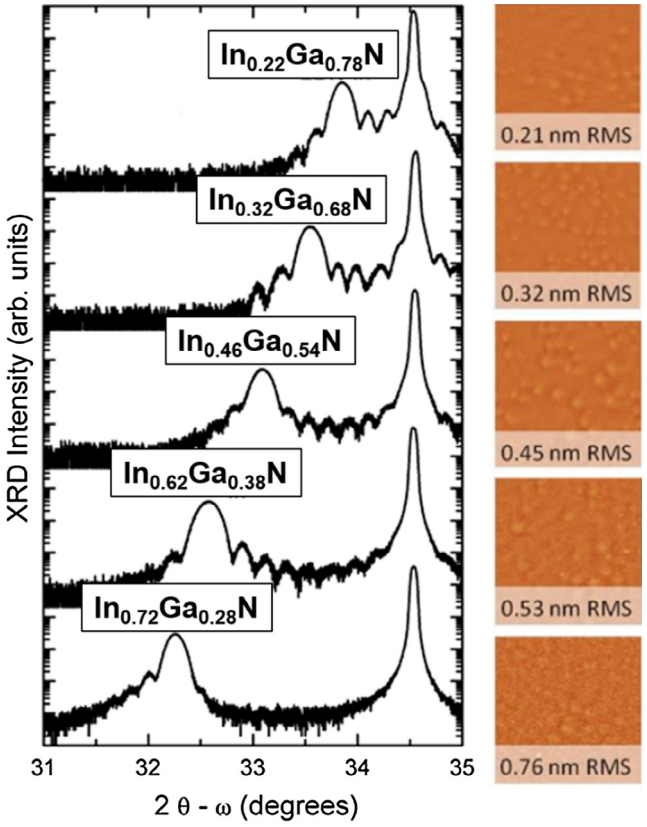

Fig. 6. X-ray diffraction and AFM of MME grown $In_xGa_{1-x}N$ films throughout the miscibility gap. Samples are all ~50 nm thick. AFM scans are 5 μm × 5 μm with a height range of 10 nm [22].

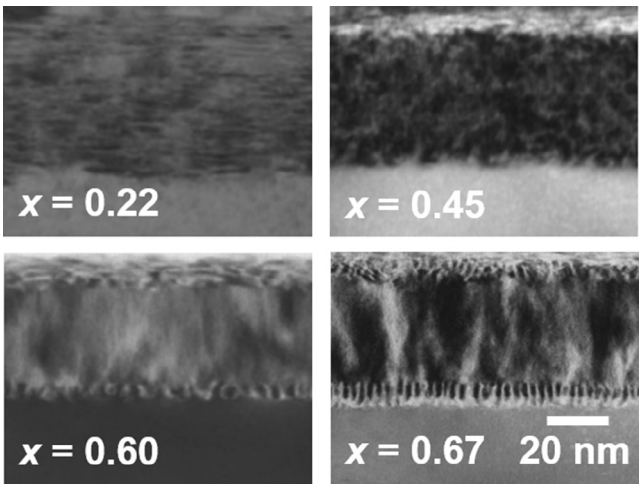

Fig. 7. TEM images of MME grown $In_xGa_{1-x}N$ films with different indium contents. The lowest indium content film demonstrates high levels of stacking faults, while the highest indium content film demonstrates moiré fringes which are misfit dislocations and can indicate immediate relaxation [38].

film and allow for a strain-free growth of the film, which reduces the number of stacking faults and threading dislocation density in the volume of the film. The x = 0.67 film is verified to have the fewest non-radiative recombination centers by exhibiting the strongest low temperature photoluminescence (PL) peak intensity at 10 K [38].

The MME growth technique is capable of growing smooth, single phase, and structurally uniform films throughout the miscibility gap. Unfortunately, due to excessive defect densities common to other MBE heteroepitaxy [14], simply growing thin $In_xGa_{1-x}N$ films with this technique is not a solution for devices requiring $In_xGa_{1-x}N$ active layers with indium contents <~67%. In order to incorporate higher quality and lower indium bearing material into device structures, more advanced nucleation and immediate strain relaxation techniques must be combined with the MME growth technique to reduce the defect density in the $In_xGa_{1-x}N$ film. Alternatively, the low temperature N-rich growth approach can be implemented.

3.4. Low temperature N-rich $In_xGa_{1-x}N$ films throughout the miscibility gap

As discussed previously, MME is an appropriate technique for growing single phase $In_xGa_{1-x}N$ of all compositions, but the defect structures present in these films, which are common in most MBE films, limit optical performance to x > 0.60. With the addition of buffer layers or other strain engineering techniques, low indium content MME $In_xGa_{1-x}N$ films with fewer non-radiative recombination centers may be achievable. Alternatively, N-rich films with III/V ≈ 0.9 and low substrate temperatures of 360–450 °C can achieve optically active films for $In_xGa_{1-x}N$ from 0 < x < 1 on GaN substrates without additional buffer layers or strain engineering [23]. This growth technique simply involves opening the plasma and metal shutters for the duration of the $In_xGa_{1-x}N$ growth, but utilizes non-traditional, low substrate temperatures [23].

Fig. 8 illustrates how the low temperature, N-rich growth technique can be implemented to grow $In_xGa_{1-x}N$ films throughout the miscibility gap [23]. These films are all single-phase and smooth, exhibiting roughness values of <1 nm RMS. The films grown with this technique at low indium contents show reduced stacking fault densities compared to that of films grown with the MME technique, as shown in Figs. 7 and 9.

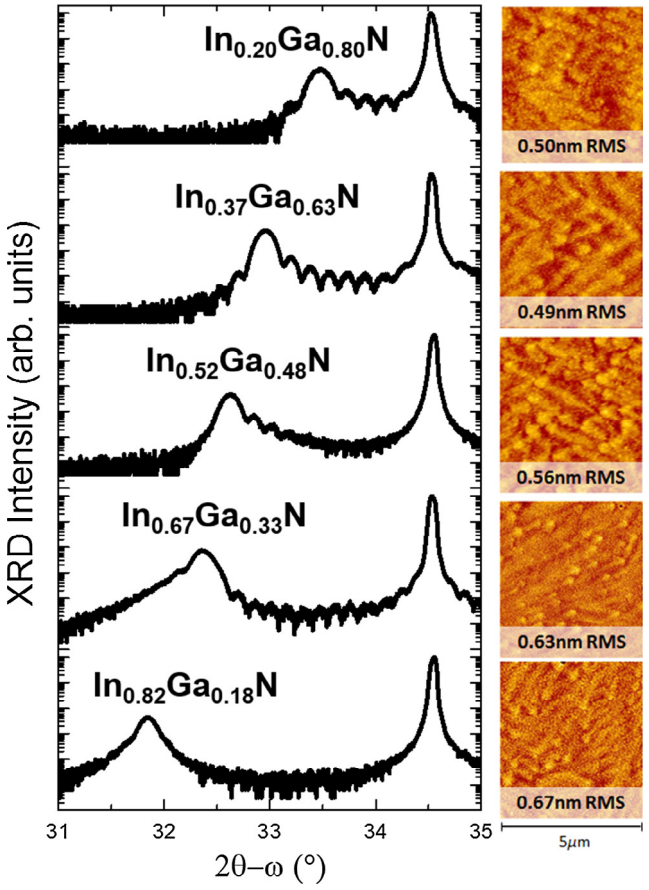

Fig. 8. X-ray diffraction and AFM of low temperature N-rich grown $In_xGa_{1-x}N$ films throughout the miscibility gap. Samples are all ~50 nm thick. AFM scans are 5 μm × 5 μm with a height range of 10 nm [23].

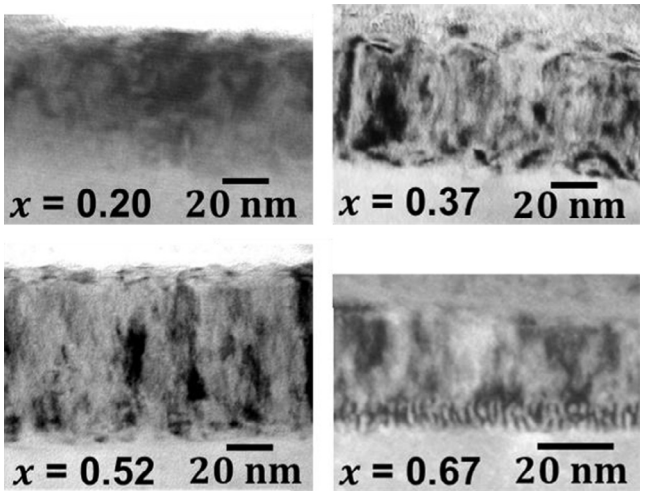

Fig. 9. TEM images of low temperature N-rich grown $In_xGa_{1-x}N$ films with different indium contents. The lowest indium content film does not show a high density of stacking faults. The highest indium composition film exhibits moiré fringes from misfit dislocations and immediate relaxation [23].

The low temperature N-rich grown $In_xGa_{1-x}N$ film with x = 0.20, shown in Fig. 9, is free of the large density of stacking faults that are seen in the MME grown film at a similar composition [23]. This noticeably different result is related to delaying the onset of relaxation. Even though the film is above the classi-

cally predicted critical thickness, the N-rich grown film is completely strained to the GaN template. The lack of significant relaxation, presumably due to the inability of dislocations to move at the low growth temperatures, results in a film with fewer defects and strong optical emission. Although this extension of the expected critical thickness occurred for the lowest indium content film and none of the N-rich films showed stacking faults, a similar strain relaxation trend is observed for both techniques. Most interesting is the onset of moiré fringes for the N-rich films is around the same composition of $x > 0.6$ when compared to the MME grown films. These moiré fringes have been shown to relate to the composition for which the critical thickness is ~1 monolayer [38]. At this composition, the strain energy is greater than the plastic deformation potential, which is the energy needed to create dislocations and relax the film. However, since the material is only 1 monolayer thick, the lack of volume causes the film to relax by creating misfit dislocation loops in the 1 monolayer plane. Subsequent material grown on this misfit layer demonstrates lower dislocation densities since the misfit dislocation network has relieved the strain.

Fig. 10 shows $(10\bar{1}5)$ X-ray diffraction reciprocal space map (RSM) XRD data for these N-rich films. The solid red line drawn on top of the image indicates where an $In_xGa_{1-x}N$ film's peak would be positioned if it was fully strained to the underlying GaN film. The dashed green line drawn on top of the image indicates where an $In_xGa_{1-x}N$ film's peak would be positioned if it was fully relaxed. The graph clearly indicates that the $In_{0.20}Ga_{0.80}N$ film is fully strained to the GaN substrate even though it is well beyond the classical critical thickness. The $In_{0.67}Ga_{0.33}N$ film is fully relaxed. Although many groups have investigated the critical thickness for complete relaxation for $In_xGa_{1-x}N$ films grown on GaN, they all predict complete relaxation for these compositions at a thickness of ~50 nm [39–42]. The XRD RSM of the $In_{0.20}Ga_{0.80}N$ film helps frame the TEM data of Fig. 9 and explains that the lack of stacking faults is due to the residual strain in the N-rich film, or the lack of relaxation generating defects. Because each of these low temperature grown films is only partially relaxed, each film has less dislocations than traditional MBE films [14], as well as MME films, and show higher optical emission [23]. This technique is more suitable for thin films than thick films as the roughness quickly increases with increasing thickness due to the limited surface mobility of metal adatoms at low temperatures.

MME and N-rich growth techniques can be separately employed to optimize III-N device performance. MME can provide smooth films at any thickness, as well as highly doped GaN and $In_xGa_{1-x}N$ films spanning the miscibility gap [22] but has limitations mostly due to high defect densities and low optical emission for $x < 0.60$. Alternatively, low temperature N-rich growth can similarly result in $In_xGa_{1-x}N$ films spanning the miscibility gap [23] with strain extending to thicker films and to higher percentages of indium resulting in reduced defect density and higher optical emission. Unfortunately, low temperature N-rich $In_xGa_{1-x}N$ is only useful in devices of sufficiently thin active regions due to the tendency of surfaces to roughen as the film thickness increases.

3.5. $In_xGa_{1-x}N$/GaN double heterojunction solar cells

Solar cells with $In_xGa_{1-x}N$ active layers have been modeled and simulated to show promising conversion efficiencies even when incorporating presently achievable material properties [43]. Although these results are promising, the lack of high magnesium p-type doping, high threading dislocation densities, and polarization fields have limited cell performance to <~2% conversion efficiency [44–47]. Magnesium doping is limited due to the large activation energy, residual donor compensation, and low solubility which when exceeded, results in a severely degraded and compensated film [48,49]. Threading dislocations from the large lattice mismatch between $In_xGa_{1-x}N$ and GaN can act as shunt paths and non-radiative recombination centers [50,51]. Due to these material concerns, limiting the overall thickness of the solar cell $In_xGa_{1-x}N$ absorber region is prudent. Thus, an n-GaN/i-$In_xGa_{1-x}N$/p-GaN double heterojunction (DHJ) device is most presently feasible, because it does not require p-type doping of the $In_xGa_{1-x}N$ absorbing layer. Unfortunately, this device structure is still severely limited due to the polarization fields at the $In_xGa_{1-x}N$/GaN interfaces that limit carrier extraction [52–54].

$In_xGa_{1-x}N$ DHJ solar cells were grown using the low temperature, N-rich method [25]. The n- and p-type GaN layers were grown with the MME growth technique, while the $In_xGa_{1-x}N$ active layer was grown with the low temperature, N-rich growth technique. As seen in Fig. 11, four different samples with either thin or thick $In_xGa_{1-x}N$ and with $x = 0.10$ or 0.20 were fabricated into solar cells. What is noteworthy is that the thickness of both active layers with $x = 0.20$ are beyond the classical critical thick-

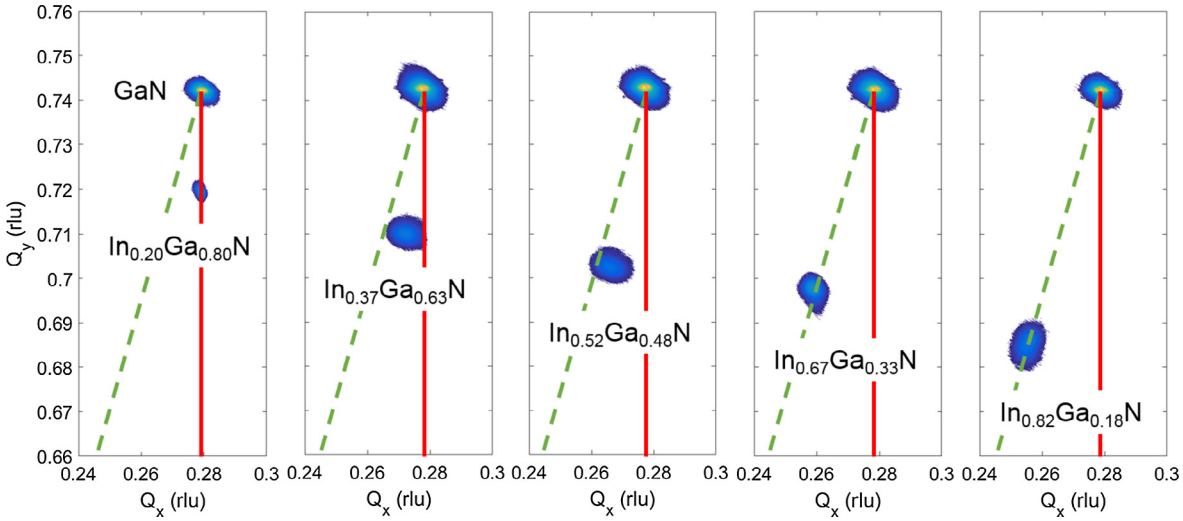

Fig. 10. $(10\bar{1}5)$ asymmetrical reciprocal space maps (RSMs) of $In_xGa_{1-x}N$ films with varying indium content on GaN substrates. Solid red and dashed green lines indicate where an $In_xGa_{1-x}N$ film peak would be positioned if it was fully strained or fully relaxed, respectively [23].

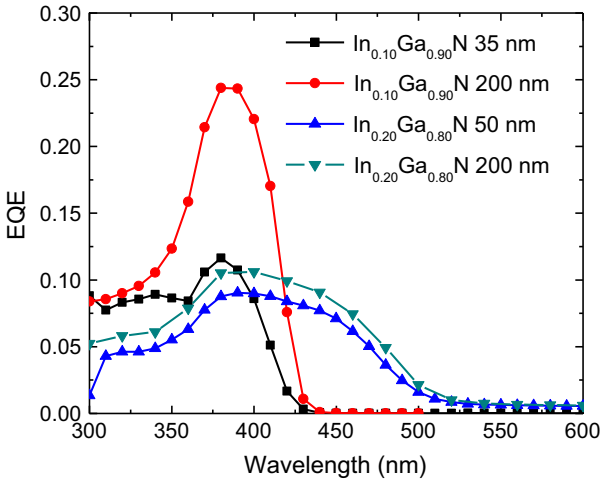

Fig. 11. $In_xGa_{1-x}N$/GaN DHJ solar cell results for both thin and thick x = 0.10 and x = 0.20 $In_xGa_{1-x}N$ layers. External quantum efficiency (EQE) vs. wavelength indicates a photovoltaic response at long wavelengths [25].

ness. This has previously prevented all solar cells reported in the literature from operating at this high of indium content. However, by impeding the dislocation movement that facilitates strain relaxation, each of the solar cells with x = 0.20 have spectral responses and a photovoltaic response well beyond what has been previously possible. While an improvement over previous limitations, much work is needed to further improve the overall efficiencies, which are not presently competitive with other solar materials.

3.6. Thick $In_xGa_{1-x}N$ buffer layers: towards a template for optoelectronic devices

In order to mitigate the effects of polarization, and isolate defects from the active region of a device, thick $In_xGa_{1-x}N$ buffer layers or templates are desirable. Additionally, for solar cell devices, homojunction devices must be implemented to improve conversion efficiencies beyond that possible with double heterojunctions [24].

Thick $In_xGa_{1-x}N$ buffer layers can provide a completely relaxed $In_xGa_{1-x}N$ film, which allows for active regions to be many hundred nanometers or microns from non-radiative recombination centers that are generated from the lattice-mismatched interface. Fig. 12 demonstrates this effect. The bottom graph depicts the XRD $(10\bar{1}5)$ FWHM for $In_{0.25}Ga_{0.75}N$ films vs. thickness. As the thickness increases, the film generates defects from relaxation and then annihilates them as the film grows thicker. A matching schematic of this process is shown in the upper pane of Fig. 12 where the film is strained before the critical thickness (extended by the use of low temperature methods) is reached and then undergoes plastic deformation which leads to defect generation. The defect density is then reduced as the film grows thicker. It is desirable to grow films even thicker and thus, reduce the defect density in the relaxed layers even more. However, the increasing roughness of the films places a technological challenge to grow these N-rich films beyond 800 nm. This is the focus of ongoing research.

4. Conclusions

The MME and low temperature N-rich approaches for the purpose of defect reduction in $In_xGa_{1-x}N$ films are described and are capable of growing $In_xGa_{1-x}N$ throughout the miscibility gap. MME films remain smooth at all thicknesses but show device quality material primarily for x < 0.20 and x > 0.60. Low temperature, N-rich films show a critical thickness extend well beyond the theoretical value which results in delaying the onset of relaxation in the range of 0.20 < x < 0.60, necessary for LED and solar cell applications. This reduced defect density results in improved optical emission but due to increased roughening with increased thickness, low temperature N-rich films are limited to thin layers. Future thick $In_xGa_{1-x}N$ substrates, or templates, are necessary to increase design freedom, as well as improve optoelectronic device performance.

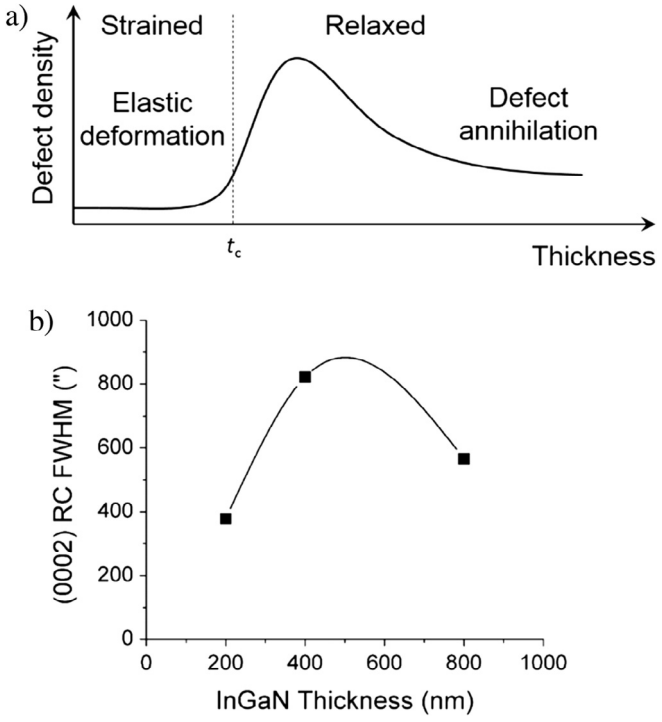

Fig. 12. (a) Schematic of defect density evolution with thickness for lattice-mismatched growth, and (b) X-ray $(10\bar{1}5)$ RC FWHM when growing $In_{0.25}Ga_{0.75}N$ at different thicknesses on a lattice-mismatched GaN substrate.

Acknowledgement

This work was supported in part by the National Science Foundation (NSF) and the Department of Energy under Grant NSF CA EEC-1041895 and in part by the Advanced Research Projects Agency-Energy, U.S. Department of Energy, under Award DE-AR0000470. Any opinions, findings, and conclusions or recommendations expressed in this material are those of the author(s) and do not necessarily reflect those of the National Science Foundation or the Department of Energy.

References

[1] Mishra BUK, Shen L, Kazior TE, Wu Y. GaN-based RF power devices and amplifiers_04414367.pdf. 2008;96(2):287–305.
[2] Neufeld CJ, Toledo NG, Cruz SC, Iza M, DenBaars SP, Mishra UK. High quantum efficiency InGaN/GaN solar cells with 2.95 eV band gap. Appl Phys Lett 2008;93 (14):91–4. <http://aip.scitation.org/doi/pdf/10.1063/1.2988894>.
[3] Xing H, Keller S, Wu Y-F, McCarthy L, Smorchkova IP, Buttari D, et al. Gallium nitride based transistors. J Phys Condens Matter 2001;13(32):7139–57. Available from: <http://stacks.iop.org/0953-8984/13/i=32/a=317?key=crossref.065dc4cbe1d37cf2a3630e15e560da3b> [cited 2017 Jan 30]..
[4] Akasaki I. Key inventions in the history of nitride-based blue LED and LD. J Cryst Growth 2007;300(1):2–10.
[5] Mukai T, Nagahama S, Kozaki T, Sano M, Morita D, Yanamoto T, et al. Current status and future prospects of GaN-based LEDs and LDs. Phys Stat Sol 2004;201

(12):2712–6. Available from: <http://doi.wiley.com/10.1002/pssa.200405113> [cited 2017 Jan 30]..
[6] Wu J. When group-III nitrides go infrared: new properties and perspectives. J Appl Phys 2009;106(1):11101. Available from: <http://aip.scitation.org/doi/10.1063/1.3155798> [cited 2017 Jan 30]..
[7] Wu J, Walukiewicz W, Yu KM, Shan W, Ager JW, Haller EE, et al. Superior radiation resistance of $In_{1-x}Ga_xN$ alloys: full-solar-spectrum photovoltaic material system. J Appl Phys 2003;94(10):6477–82. Available from: http://aip.scitation.org/doi/pdf/10.1063/1.1618353.
[8] Nakamura S. Nobel Lecture: Background story of the invention of efficient blue InGaN light emitting diodes. Rev Mod Phys 2015;87(4):1139–51. Available from: <http://link.aps.org/doi/10.1103/RevModPhys.87.1139> [cited 2017 Jan 30].
[9] Singh R, Doppalapudi D, Moustakas TD, Romano LT. Phase separation in InGaN thick films and formation of InGaN/GaN double heterostructures in the entire alloy composition; 1998. <http://oasc12039247realmedia.com/RealMedia/ads/click_lx.ads/www.aip.org/pt/adcenter/pdfcover_test/L-37/1767098002/x01/AIP-PT/APL_ArticleDL_0117/NeedleInHaystack_1640x440.jpg/434f71374e315a556e61414141774c75?x>.
[10] Moseley M, Gunning B, Greenlee J, Lowder J, Namkoong G, Alan Doolittle W. Observation and control of the surface kinetics of InGaN for the elimination of phase separation. J Appl Phys 2012;112(1). Available from: <http://aip.scitation.org/doi/pdf/10.1063/1.4733347>.
[11] Stringfellow GB. Microstructures produced during the epitaxial growth of InGaN alloys. J Cryst Growth 2010;312(6):735–49.
[12] Nanishi Y, Saito Y, Yamaguchi T. RF-Molecular beam epitaxy growth and properties of InN and related alloys. Jpn J Appl Phys 2003;42(Part 1, No. 5A):2549–59. Available from: <http://stacks.iop.org/1347-4065/42/2549> [cited 2017 Jan 31].
[13] Yam FK, Hassan Z. InGaN: an overview of the growth kinetics, physical properties and emission mechanisms. Superlatt Microstruct 2008;43(1):1–23.
[14] Heying B, Averbeck R, Chen LF, Haus E, Riechert H, Speck JS. Control of GaN surface morphologies using plasma-assisted molecular beam epitaxy; 2000. <http://oasc12039247realmedia.com/RealMedia/ads/click_lx.ads/www.aip.org/pt/adcenter/pdfcover_test/L-37/1952595056/x01/AIP-PT/JAP_ArticleDL_0117/AIP-2968_JAP_1640x440r2.jpg/434f71374e315a556e61414141774c75?x>.
[15] Namkoong G, Trybus E, Lee KK, Moseley M, Doolittle WA, Look DC. Metal modulation epitaxy growth for extremely high hole concentrations above 10^{19} cm^{-3} in GaN. Appl Phys Lett 2008;93(17):17–20. Available from: http://aip.scitation.org/doi/pdf/10.1063/1.3005640.
[16] Moseley M, Billingsley D, Henderson W, Trybus E, Doolittle WA. Transient atomic behavior and surface kinetics of GaN. J Appl Phys 2009;106(1). Available from: <http://aip.scitation.org/doi/pdf/10.1063/1.3148275>.
[17] Gunning B, Lowder J, Moseley M, Alan Doolittle W. Negligible carrier freeze-out facilitated by impurity band conduction in highly p-type GaN. Appl Phys Lett 2012;101(8):82106. Available from: <http://aip.scitation.org/doi/10.1063/1.4747466> [cited 2017 Jan 25].
[18] Gunning BP, Fabien CAM, Merola JJ, Clinton EA, Doolittle WA, Wang S, et al. Comprehensive study of the electronic and optical behavior of highly degenerate p-type Mg-doped GaN and AlGaN. J Appl Phys 2015;117(4). http://dx.doi.org/10.1063/1.4906464.
[19] Burnham SD, Namkoong G, Look DC, Clafin B, Doolittle WA. Reproducible increased Mg incorporation and large hole concentration in GaN using metal modulated epitaxy. J Appl Phys 2008;104(2):24902. Available from: <http://link.aip.org/link/JAPIAU/v104/i2/p024902/s1&Agg=doi> [cited 2014 Feb 18].
[20] Moseley M, Lowder J, Billingsley D, Doolittle WA. Control of surface adatom kinetics for the growth of high-indium content InGaN throughout the miscibility gap. Appl Phys Lett 2010;97(19):1–4. Available from: <http://aip.scitation.org/doi/pdf/10.1063/1.3509416>.
[21] Moseley M, Gunning B, Greenlee J, Lowder J, Namkoong G, Alan Doolittle W. Observation and control of the surface kinetics of InGaN for the elimination of phase separation. J Appl Phys 2012;112(1):14909. Available from: <http://link.aip.org/link/JAPIAU/v112/i1/p014909/s1&Agg=doi> [cited 2014 Feb 18].
[22] Moseley M, Lowder J, Billingsley D, Doolittle WA. Control of surface adatom kinetics for the growth of high-indium content InGaN throughout the miscibility gap. Appl Phys Lett 2010;97(19):191902. Available from: <http://link.aip.org/link/APPLAB/v97/i19/p191902/s1&Agg=doi> [cited 2014 Feb 18].
[23] Fabien CAM, Gunning BP, Alan Doolittle W, Fischer AM, Wei YO, Xie H, et al. Low-temperature growth of InGaN films over the entire composition range by MBE. J Cryst Growth 2015;425:115–8. http://dx.doi.org/10.1016/j.jcrysgro.2015.02.014.
[24] Fabien CAM, Doolittle WA. Guidelines and limitations for the design of high-efficiency InGaN single-junction solar cells. Sol Energy Mater Sol Cells 2014;130:354–63. http://dx.doi.org/10.1016/j.solmat.2014.07.018.
[25] Fabien CAM, Maros A, Honsberg CB, Doolittle WA. III-nitride double-heterojunction solar cells with high In-content InGaN absorbing layers: comparison of large-area and small-area devices. IEEE J Photovolt 2016;6(2):460–4.
[26] Burnham SD, Alan Doolittle W, Namkoong G, Henderson W. Mg doped GaN using a valved, thermally energetic source: enhanced incorporation, control and quantitative optimization. MRS Proc 2003;798:Y8.11. Available from: <http://journals.cambridge.org/abstract_S1946427400107432>.
[27] Namkoong G, Doolittle WA, Brown AS, Losurdo M, Capezzuto P, Bruno G. Role of sapphire nitridation temperature on GaN growth by plasma assisted molecular beam epitaxy: Part I. Impact of the nitridation chemistry on material characteristics. J Appl Phys 2002;91(4):2499–507. Available from: <http://aip.scitation.org/doi/10.1063/1.1435834> [cited 2017 Jan 25].
[28] Losurdo M, Capezzuto P, Bruno G, Namkoong G, Doolittle WA, Brown AS. Role of sapphire nitridation temperature on GaN growth by plasma assisted molecular beam epitaxy: Part II. Interplay between chemistry and structure of layers. J Appl Phys 2002;91(4):2508–18. Available from: <http://aip.scitation.org/doi/10.1063/1.1435835> [cited 2017 Jan 25].
[29] Gunning BP, Clinton EA, Merola JJ, Doolittle WA, Bresnahan RC. Control of ion content and nitrogen species using a mixed chemistry plasma for GaN grown at extremely high growth rates >9 μm/h by plasma-assisted molecular beam epitaxy. J Appl Phys 2015;118(15):155302. Available from: <http://scitation.aip.org/content/aip/journal/jap/118/15/10.1063/1.4933278>.
[30] Burnham SD, Alan Doolittle W. In situ growth regime characterization of AlN using reflection high energy electron diffraction. J Vac Sci Technol B Microelectron Nanom Struct 2006;24(4):2100. Available from: <http://scitation.aip.org/content/avs/journal/jvstb/24/4/10.1116/1.2219757> [cited 2017 Jan 31].
[31] Burnham SD, Namkoong G, Lee K-K, Doolittle WA. Reproducible reflection high energy electron diffraction signatures for improvement of AlN using in situ growth regime characterization. J Vac Sci Technol B Microelectron Nanom Struct 2007;25(3):1009. Available from: <http://scitation.aip.org/content/avs/journal/jvstb/25/3/10.1116/1.2737435> [cited 2017 Jan 31].
[32] Moseley M, Gunning B, Lowder J, Alan Doolittle W, Namkoong G. Structural and electrical characterization of InN, InGaN, and p-InGaN grown by metal-modulated epitaxy. J Vac Sci Technol B, Nanotechnol Microelectron Mater Process Meas Phenom 2013;31(3):03C104. Available from: <http://avs.scitation.org/doi/10.1116/1.4790865> [cited 2017 Jan 31].
[33] Trybus E, Namkoong G, Henderson W, Burnham S, Doolittle WA, Cheung M, et al. InN: a material with photovoltaic promise and challenges. J Cryst Growth 2006;288(2):218–24.
[34] Trybus E, Jani O, Burnham S, Ferguson I, Honsberg C, Steiner M, et al. Characteristics of InGaN designed for photovoltaic applications. Phys Status Solidi 2008;5(6):1843–5. Available from: <http://doi.wiley.com/10.1002/pssc.200778693>.
[35] Thaler GT, Koleske DD, Lee SR, Bogart KHA, Crawford MH. Thermal stability of thin InGaN films on GaN. J Cryst Growth 2010;312(11):1817–22.
[36] Stanley I, Coleiny G, Venkat R. Theoretical study of In desorption and segregation kinetics in MBE growth of InGaAs and InGaN. J Cryst Growth 2003;251(1):23–8.
[37] Adelmann C, Langer R, Feuillet G, Daudin B. Indium incorporation during the growth of InGaN by molecular-beam epitaxy studied by reflection high-energy electron diffraction intensity oscillations; 1999. <http://oasc12039247realmedia.com/RealMedia/ads/click_lx.ads/www.aip.org/pt/adcenter/pdfcover_test/L-37/1767098002/x01/AIP-PT/APL_ArticleDL_0117/NeedleInHaystack_1640x440.jpg/434f71374e315a556e61414141774c75?x>.
[38] Fischer AM, Wei YO, Ponce FA, Moseley M, Gunning B, Doolittle WA. Highly luminescent, high-indium-content InGaN film with uniform composition and full misfit-strain relaxation. Appl Phys Lett 2013;103(13):131101. Available from: <http://link.aip.org/link/APPLAB/v103/i13/p131101/s1&Agg=doi> [cited 2014 Feb 18].
[39] People R, Bean JC. Calculation of critical layer thickness versus lattice mismatch for Ge_xSi_{1-x}/Si strained-layer heterostructures. Appl Phys Lett 1985;47(3):322–4. Available from: <http://aip.scitation.org/doi/10.1063/1.96206> [cited 2017 Jan 30].
[40] Srinivasan S, Geng L, Liu R, Ponce FA, Narukawa Y, Tanaka S. Slip systems and misfit dislocations in InGaN epilayers. Appl Phys Lett 2003; 83(25): 5187–9. Available from: <http://aip.scitation.org/doi/10.1063/1.1633029> [cited 2017 Jan 30].
[41] Matthews JW, Mader S, Light TB. Accommodation of misfit across the interface between crystals of semiconducting elements or compounds. J Appl Phys 1970;41(9):3800–4. Available from: <http://aip.scitation.org/doi/10.1063/1.1659510> [cited 2017 Jan 30].
[42] Fischer A, Kühne H, Richter H. New approach in equilibrium theory for strained layer relaxation. Phys Rev Lett 1994;73(20):2712–5. Available from: <http://link.aps.org/doi/10.1103/PhysRevLett.73.2712>. [cited 2017 Jan 30].
[43] Fabien CAM, Moseley M, Gunning B, Doolittle WA, Fischer AM, Wei YO, et al. Simulations, practical limitations, and novel growth technology for InGaN-based solar cells. IEEE J Photovolt 2014;4(2):601–6. Available from: <http://ieeexplore.ieee.org/document/6683005/> [cited 2017 Jan 25].
[44] Lang JR, Neufeld CJ, Hurni CA, Cruz SC, Matioli E, Mishra UK, et al. High external quantum efficiency and fill-factor InGaN/GaN heterojunction solar cells grown by NH3-based molecular beam epitaxy. Appl Phys Lett 2011;98(13):131115. Available from: <http://aip.scitation.org/doi/10.1063/1.3575563> [cited 2017 Jan 30].
[45] Matioli E, Neufeld C, Iza M, Cruz SC, Al-Heji AA, Chen X, et al. High internal and external quantum efficiency InGaN/GaN solar cells. Appl Phys Lett 2011;98(2):21102. Available from: <http://aip.scitation.org/doi/10.1063/1.3540501> [cited 2017 Jan 30].
[46] Sang L, Liao M, Ikeda N, Koide Y, Sumiya M. Enhanced performance of InGaN solar cell by using a super-thin AlN interlayer. Appl Phys Lett 2011;99(16):161109. Available from: <http://aip.scitation.org/doi/10.1063/1.3654155> [cited 2017 Jan 30].
[47] Cai X, Zeng S, Zhang B. Fabrication and characterization of InGaN p-i-n homojunction solar cell. Appl Phys Lett 2009;95(17):173504. Available from: <http://aip.scitation.org/doi/10.1063/1.3254215> [cited 2017 Jan 30].

[48] Pantha BN, Wang H, Khan N, Lin JY, Jiang HX. Origin of background electron concentration in $In_xGa_{1-x}N$ alloys. Phys Rev B 2011;84(7):75327. Available from: <http://link.aps.org/doi/10.1103/PhysRevB.84.075327> [cited 2017 Jan 30].
[49] Van de Walle CG, Stampfl C, Neugebauer J. Theory of doping and defects in III–V nitrides. J Cryst Growth 1998;189:505–10.
[50] Kozodoy P, Ibbetson JP, Marchand H, Fini PT, Keller S, Speck JS, et al. Electrical characterization of GaN p-n junctions with and without threading dislocations; 1998. <http://oasc12039247realmedia.com/RealMedia/ads/click_lx.ads/www.aip.org/pt/adcenter/pdfcover_test/L-37/1767098002/x01/AIP-PT/APL_ArticleDL_0117/NeedleInHaystack_1640x440.jpg/434f71374e315a556e61414141774c75?x>.
[51] Abell J, Moustakas TD. The role of dislocations as nonradiative recombination centers in InGaN quantum wells. Appl Phys Lett 2008;92(9):91901. Available from: <http://aip.scitation.org/doi/10.1063/1.2889444> [cited 2017 Jan 30].
[52] Yu ET, Dang XZ, Asbeck PM, Lau SS, Sullivan GJ. Spontaneous and piezoelectric polarization effects in III–V nitride heterostructures. J Vac Sci Technol B Microelectron Nanom Struct Process Meas Phenom; 1999.
[53] Li ZQ, Lestradet M, Xiao YG, Li S. Effects of polarization charge on the photovoltaic properties of InGaN solar cells. Phys Status Solidi 2011;208(4):928–31. Available from: <http://doi.wiley.com/10.1002/pssa.201026489> [cited 2017 Jan 30].
[54] Chang J-Y, Kuo Y-K. Numerical Study on the Influence of Piezoelectric Polarization on the Performance of p-on-n (0001)-Face GaN/InGaN p-i-n Solar Cells. IEEE Electron Device Lett. 2011;32(7):937–9. Available from: <http://ieeexplore.ieee.org/document/5773076/> [cited 2017 Jan 30].

Evan A. Clinton received the M.S. degree in electrical engineering from the Georgia Institute of Technology, Atlanta, Georgia, USA, in 2015, where he is currently working toward a Ph.D. degree. His research interests include plasma enhanced molecular beam epitaxy of III-Nitrides to improve electronic and optoelectronic devices.

Dr. Alan Doolittle is a professor in the School of Electrical and Computer Engineering at Georgia Institute of Technology. His principal interest is in the development of nitride-based and crystalline oxide-based devices as well as applying new growth techniques to facilitate material and device improvements. He has authored/co-authored over 118 research papers and 101 presentations (34 invited) as well as numerous technical reports and patents. He has received numerous awards including a 2004 NSF CAREER, 2003 Ga Tech Faculty of the Year award, the 2005 ECE Outstanding Junior Faculty Member Award, the 2005 Lockheed Martin Aeronautics Company's Dean's Award for Teaching Excellence, and the 2008 Ga Tech Outstanding Achievement in Research Program Development Award. His research interests have centered on plasma enhanced molecular beam epitaxy for III-Nitride and complex oxide growth for electronic, optoelectronic devices and neuromorphic computational devices.